Surface & Coatings Technology 205 (2010) 57–65

Contents lists available at ScienceDirect

Surface & Coatings Technology

journal homepage: www.elsevier.com/locate/surfcoat

Microstructural evolution of 7 wt.% Y_2O_3–ZrO_2 thermal barrier coatings due to stress relaxation at elevated temperatures and the concomitant changes in thermal conductivity

Chris Petorak [c], Jan Ilavsky [a], Hsin Wang [b], Wally Porter [b], Rodney Trice [c,*]

[a] Argonne National Lab, United States
[b] Oak Ridge National Lab, United States
[c] Purdue University, School of Materials Engineering, United States

ARTICLE INFO

Article history:
Received 18 March 2010
Accepted in revised form 1 June 2010
Available online 9 June 2010

Keywords:
Plasma spray
YSZ
Thermal barrier coatings
Stress relaxation
Small angle neutron scattering
Mechanical properties

ABSTRACT

The purpose of this study was to evaluate the combined effect of stress and temperature on the microstructure of air plasma-sprayed 7 wt.% Y_2O_3–ZrO_2 thermal barrier coatings, and relate microstructural changes to the thermal conductivity, k_{th}. To simulate TBC service conditions, stand-alone tubes of YSZ were stress relaxed, starting from a compressive stress of 60 MPa, at temperatures of 1000 °C or 1200 °C. The duration of the stress relaxation test was either 5 min or 3 h. Detailed scanning electron microscopy (SEM) and Porod's specific surface area (SSA) analysis of small angle neutron scattering (SANS) results were used to determine which void systems, either interlamellar pores or intralamellar cracks, contributed to the observed relaxation of stress in the coatings. SEM investigations revealed closure of intralamellar cracks located perpendicular to the stress direction. For thinner YSZ coatings, SANS measurements indicated a statistically significant reduction in the total SSA and SSA associated with intralamellar cracks after stress relaxation at the times, temperatures, and stress investigated compared to those samples that were exposed to identical times and temperatures, but no stress. The SSA associated with the interlamellar pores was not significantly smaller in YSZ coatings stress relaxed from 60 MPa at 1200 °C for 3 h compared to as-sprayed coatings. The thermal conductivity of the coatings was strongly influenced by stress, with increases in k_{th} observed after only 5 min at 60 MPa and 1200 °C. Reductions in the total SSA were directly linked to increases in k_{th}.

1. Introduction

Air plasma-sprayed (APS) thermal barrier coatings comprised of 7 wt.% Y_2O_3–ZrO_2 or YSZ are used in high-temperature applications to protect underlying metallic structure in gas turbines. The as-sprayed coating has a lamellar microstructure made up of multiple stacked individual lamellae that are produced as droplets of molten YSZ impact the substrate [1–4]. The presence of oxygen vacancies in the YSZ, along with the phonon scattering network of interlamellar pores and intralamellar cracks that comprise the stacked lamella, provide significant thermal protection. Ellipse-shaped interlamellar pores are located between lamella, with the long axis of the pore typically perpendicular to the spray direction. Intralamellar cracks divide individual lamella into smaller sections, and are oriented parallel to the spray direction. With service temperatures ranging from 800 °C to 1200 °C, sintering of the pores and cracks is known to occur. More specifically, small angle neutron scattering (SANS) showed that the specific surface area of the intralamellar cracks rapidly decreases for heat treatments up to 1000 °C. The SSA of the interlamellar pores is reduced, beginning at heat treatments of 1100 °C and greater [5]. These changes in microstructure have been observed in AFM images after heat treatments [6] and linked to increases in thermal conductivity [7].

In addition to the temperature, large in-plane compressive stresses develop due to a thermal mismatch between the coating and substrate. The large in-plane compressive stresses relax with time at temperature, and have been documented for a number of applied stresses, test temperatures, and initial coating conditions previously [8–11]. Plasma-sprayed coatings express a two regime stress relaxation behavior, which consists of an initial fast stress relaxation occurring during the first ten minutes of stress application followed by a slower rate of relaxation taking place during the remaining 170 min tested [10].

The inability of plasma-sprayed microstructure to recover from compressive stress relaxation due to in-plane strain during operation results in the formation of through thickness cracks, and ultimately reduced mechanical stability and shorter coating lifetimes [12–19]. While the mechanical integrity of the coating is understood, the

* Corresponding author. Neil Armstrong Hall of Engineering, 701 West Stadium Avenue, West Lafayette, IN 47907-2045, United States. Tel.: +1 765 494 6405.
E-mail address: rtrice@purdue.edu (R. Trice).

0257-8972/$ – see front matter © 2010 Elsevier B.V. All rights reserved.
doi:10.1016/j.surfcoat.2010.06.007

combined effect of temperature and stress on the microstructure and thermal conductivity of the coating has not been investigated. Thus, the purpose of the current paper is to link the microstructural evolution of air plasma-sprayed YSZ coatings that occurs during stress relaxation at representative service temperatures to the thermal conductivity of the coating. Microstructural evolution was observed using scanning electron microscopy by observing the same location in the specimen before and after stress relaxation to document changes in the intralamellar cracks. Porod's SSA analysis of small angle neutron scattering data was used to quantify changes in intralamellar crack and interlamellar pore populations. Thermal conductivity was measured using laser flash techniques on samples that were stress relaxed at elevated temperature, and samples exposed to the same temperature but no stress applied.

2. Materials and methods

2.1. Fabrication of stand-alone YSZ coatings

APS stand-alone coatings for all stress relaxation tests were produced in accordance with parameters and methods outlined in previous work [9–11] and are only briefly reviewed here. The coatings were manufactured of a fused and crushed HC-Starck Amperit 825.0 7 wt.% Y_2O_3–ZrO_2 powder with particle size range of 22.5 ± 6 μm. They were sprayed at Ames Laboratory using a Praxair SG-100 gun with a 730 anode (part number), a 729 cathode and a 113 gas injector. Cylindrical copper rods (12.7 mm in diameter) and modified aluminum rods were used as the substrates for the coatings. The shape of the modified aluminum rod is shown schematically in Fig. 1a; the approximate diameter for this geometry is 25 mm, with other dimensions noted in the figure. Generally, forty coating passes were applied as either rod type was rotated. Thicker coatings required increasing the number of coating passes. The spray controls are listed in Table 1. The coatings on the modified aluminum substrates were sprayed with the same spray parameters as the copper rods, with the exception that the direction of rotation for this rod type was reversed for half of the coating passes during the spray process. The change in rotation direction of the substrate was used to alleviate a non-uniform thick coating from forming along the flat sections of the modified geometry substrate. Samples from the copper and modified aluminum substrates, which were nominally 250 mm long, were sectioned into ~18 mm and ~25 mm lengths, respectively. The end of each cut sample was machined parallel using a diamond tool on a lathe. To produce stand-alone coatings, copper substrates were removed by etching the YSZ coatings with nitric acid; aluminum substrates were etched from the YSZ coating with hydrochloric acid. Height and coating thickness were measured using calipers. Coatings were mechanically evaluated in the as-sprayed condition or heat-treated condition of 50 h at 1000° or 1200 °C. Following stress relaxation, the flat surfaces on the modified samples made it possible to cut-out flat 14 mm diameter thermal diffusivity samples.

Table 1
Thermal spray conditions used for fabrication of YSZ coatings.

Power	37 kW
Stand-off distance	10 cm
Arc gas rate	25 slm (Ar)
Aux gas rate	21 slm (He)
Powder carrier gas rate	6 slm (Ar)

Two separate coating thicknesses were investigated. The first set of coatings investigated was ~600 μm thick; the second set of coatings was ~900 μm thick. While the thinner coatings are more representatives of conventional thermal barriers, the thicker coatings afforded small angle neutron scattering measurements from all three scattering orientations. The bulk density of all YSZ coatings was 5.52 g/cm^3, as determined by the Archimedes method. The orientation of the interlamellar pores and intralamellar cracks with respect to the sample orientation during stress relaxation testing is shown in Fig. 1b.

2.2. Stress relaxation testing of stand-alone YSZ coatings

The uniaxial compression testing configuration was chosen because it allows the entire volume of the test specimen to be subjected to the applied stress, and is representative of the stress state a coating experiences in service. As discussed in Section 2.1, standard [9,10] and modified tubular sample geometries were stress relaxed. Although not presented here, no differences in stress relaxation versus time behavior were noted between the two geometries.

High-temperature compression testing on stand-alone coating samples was performed using a servo-hydraulic load frame (MTS 810

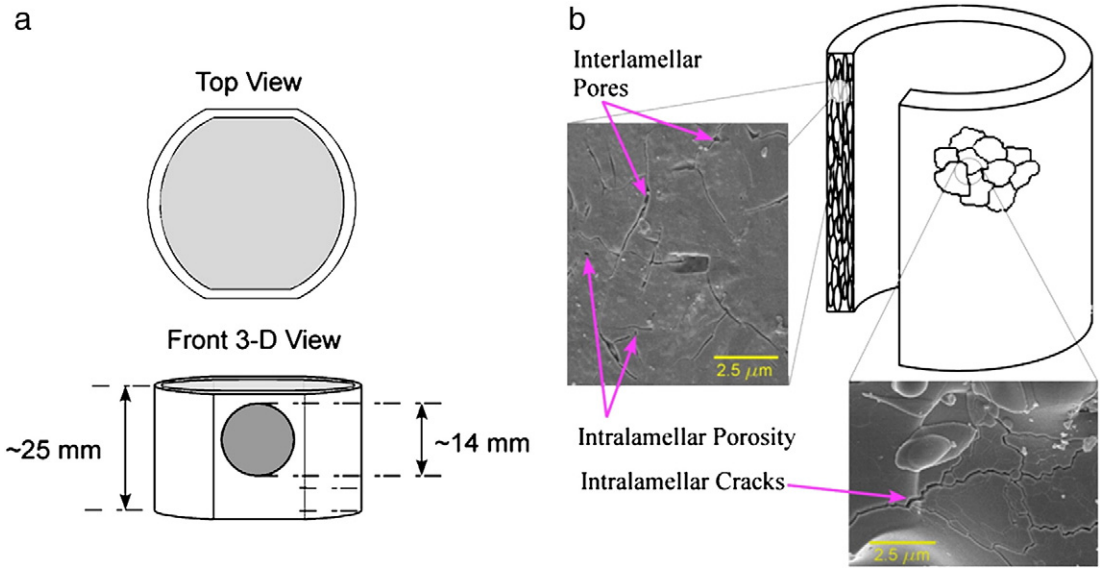

Fig. 1. (a) Stand-alone coating samples used for thermal conductivity and density measurements were sprayed first on a modified aluminum substrate that contained flat regions; the substrate was later removed, leaving the stand-alone coating. 14 mm disks were cut from these flat regions for laser flash experiments after stress relaxation testing. (b) Combination of SEM and schematic images showing a cut-a-way view of stand-alone plasma-sprayed coating with the orientation of the interlamellar pores and intralamellar cracks noted. Stress was applied uniaxially along the tube length.

Load Frame) equipped with hydraulic collet grips, an alignment fixture (MTS 609 Alignment Fixture), a 100 kN force transducer, SiC pushrods, and a high-temperature furnace (Applied Test Systems, Inc., Butler, PA). Strain was measured with a high-temperature extensometer (MTS 632.70H-01) with a resolution of ±1 μm. Alignment of the load train was performed prior to testing as is detailed in ref [10]. Stand-alone coatings were relaxed at two temperatures, 1000° and 1200 °C, from an initial applied stress of 60 MPa, for either 5 min or 3 h. Temperature and stress relaxation testing parameters were chosen to both reflect operational conditions and to coincide with our previous research on stand-alone coatings [8,11]. Stress relaxation tests that lasted only 5 min were designed to differentiate fast and slow stress relaxation mechanisms. Coatings were stress relaxed in the as-sprayed condition, and after 50 hour heat treatments at 1000 °C and 1200 °C. Surface diffusion, a non-densifying mass transport mechanism that can cause coarsening of the microstructure, is known to occur at 1000 °C. Heat treatments at 1200 °C activate densifying bulk diffusion mass transport [6].

During stress relaxation each sample was heated to the desired temperature at a rate of 10 °C/min under no applied load. After the target temperature was reached and stabilized for 15 min, the test was initiated by monotonically increasing the stress applied to the YSZ tube at a rate of 20 N/s to a pre-determined initial stress. Once the initial stress was reached, the control system of servo-hydraulic load frame was changed from force to strain feedback, and the strain was held constant for either 5 min or 3 h. For control purposes, another stand-alone sample was placed in proximity to the sample being stress relaxed, but not within the load train. Thus, the effect of temperature could be decoupled from the effect of stress.

2.3. SEM investigations of coatings

Coatings were studied using SEM (Hitachi FESEM) at the same location on the coating surface before and after stress relaxation testing. By returning to the same location, changes in microstructural features due to temperature or temperature and stress could be reliably captured. To facilitate locating the same area on a sample, stand-alone coatings were ground along their length on both sides of their surface to produce two flat surfaces 180° apart. The grind was ~2 mm in width and the flat edge allowed the coating to be mounted and remounted with the same orientation relative to the electron beam of the SEM. Coatings were inspected in the as-sprayed condition, after 5 min of stress relaxation, and after the full 180 min of stress relaxation at 1200 °C. To enhance grain structure in the YSZ coating, some samples were heat-treated for 1 h at 1000 °C prior to stress relaxation testing to thermally etch the surface. Heat treatments of YSZ at 1000 °C have been shown to activate surface diffusion, causing minor grain boundary grooving that helps provide contrast between adjacent grains [6].

2.4. Small angle neutron scattering (SANS) measurements

SANS measurements were performed at the NIST Center for Neutron Research (NCNR) [5,20,22]. A sector analysis of the 2-D detector data was carried out over 180° to evaluate anisotropy of the small angle neutron scattering associated with the anisotropy of the APS coatings microstructure. For each sector, a Porod fit was applied to the data to extract Porod constant. The fit was performed using Igor Pro software[1] and the Irena package for small angle scattering [21]. The curve fit used traditional Porod's law as given by:

$$I(Q) = PC \cdot Q^{-4} + background$$

where PC is the Porod constant, and I(Q) is the scattered intensity as a function of the scattering vector, Q. The Porod constants were plotted as a function of their azimuthal angles in a polar plot to create an apparent Porod surface plot. This plot was then used to correlate with the original anisotropy of the microstructure [5,20,22].

This 2-D apparent specific surface area plot then can be used to generate 3D distribution of apparent Porod surfaces by taking advantage of the isotropic direction in this system. The 3D apparent specific surface area distribution in the APS YSZ coatings has been shown to resemble a bulging ellipsoid. This ellipsoid can now be integrated and the quantitative specific surface area per unit volume for each void system separately as well as the total void population, is found by dividing the integrated 3-D Porod surface area by the mean difference in neutron scattering length density between the solid material and the pores [5,20,22].

Two separate SANS experiments were performed for stress relaxed coatings. Initially, a set of ~600 μm thick coatings was used to measure anisotropic scattering events from a single orientation for the sample conditions of as-sprayed, heat-treated at 1200 °C for 3 h, and stress relaxed at 1200 °C/60 MPa for 3 h. Because an applied compressive stress during relaxation could affect the isotropic scattering in the plasma-spray direction, a second thicker set of coatings, ~900 μm thick, were employed to investigate both the isotropic scattering orientation and anisotropic scattering directions. The second study was expanded to include the effects of test temperature and test duration by investigating relaxation at 1000 °C/60 MPa for 3 h, and 1200 °C/60 MPa for 5 min and for 3 h of relaxation. All relaxation conditions were compared to equivalent heat-treatment times with no applied stress.

2.5. Thermal conductivity measurements

Thermal conductivity was calculated from thermal diffusivity and specific heat measurements made in the High Temperature Materials Laboratory (HTML) at Oak Ridge National Lab, and bulk density measurements made by the Archimedes method [23] according to:

$$k = \alpha \cdot \rho \cdot c_P \cdot 100$$

where k is thermal conductivity (W/m/K), α is thermal diffusivity (cm^2/s), ρ is the bulk density (g/cm^3), and c_p is the specific heat at constant pressure (J/g/K). Thermal diffusivity was measured according to ASTM E-1461 [24]. The laser flash system at HTML employed a fiber optic laser as the energy source to measure thermal diffusivity. During testing this laser was attached to a furnace with an Ar atmosphere that contained the coating samples and an infrared (IR) detector. Because zirconia is semi-transparent to radiation with wavelengths near the IR portion of the electromagnetic spectrum [25], the top and bottom surfaces of the coating samples were completely covered with colloidal graphite prior to testing. This graphite covering absorbed the incident laser radiation so that the heat transfer through the coating took place only by conduction.

Two furnace–detector setups were used to evaluate the coating thermal diffusivity over a temperature range consistent with gas turbine operation. The first furnace featured an InSb detector and was used for measurements from 200 to 500 °C. The second furnace featured a Si detector and was used for measurements from 600 to 1200 °C. The measurements were recorded at 100 °C intervals over both temperature ranges. A computer controlled the testing procedure and automatically calculated average thermal diffusivity values from the sample thickness input by the user and three consecutive IR detector data sets collected at the measurement temperature. These calculations included corrections for radiation losses determined from the work of Clark and Taylor [26].

The thermal diffusivity was measured for coatings that were stress relaxed using the modified stand-alone coating geometry shown in Fig. 1a, and compared to equivalent heat-treatment conditions that experienced no applied loading. The temperature-dependent c_p data

[1] Wavemetrics Inc., Lake Oswego, OR.

for the YSZ was determined from differential scanning calorimetry experiments performed by researchers at HTML [27].

3. Results

3.1. Changes in density and height due to uniaxial relaxation

Table 2 lists the applied strains necessary to achieve 60 MPa of stress as a function of coating condition. The recorded standard deviation in Table 2 is at least 0.09%, based both on repeated measurements as well as the uncertainty of the calculated strain value for a single sample; in some cases this value is higher. Note that in the as-sprayed condition, a higher strain ($0.46 \pm 0.13\%$) was required to achieve 60 MPa than a coating that has been sintered at 1200 °C for 50 h prior to testing ($0.28 \pm 0.09\%$), indicating that that the sintered coatings were stiffer than the as-sprayed coatings.

The average height change represents measurements made before and after stress relaxation at 1200 °C/60 MPa/3 h. For coating conditions where the average height change is greater than the applied strain required to achieve 60 MPa it indicates that the sample was no longer in contact with the upper crosshead at some point during the 3-hr stress relaxation test. For example, the as-sprayed coating required an applied strain of $0.46 \pm 0.13\%$ to achieve a stress 60 MPa but shrunk $0.75 \pm 0.34\%$ during the test. This is consistent with stress relaxation data that indicates that as-sprayed coatings will fully relax (i.e. it will support no stress) during a 3-hr test at 1200 °C [10].

For samples heat-treated at 1000 °C for 50 h prior to testing, then stress relaxed at 1200 °C/60 MPa/3 h, the permanent change in height was less than the amount of strain required to generate the 60 MPa in the sample. Thus, at the end of 3 h not all of the initial stress was relaxed. The average height change in the sample heat-treated for 50 h at 1200 °C prior to testing was only $0.18 \pm 0.09\%$ as compared to the applied strain of $0.28 \pm 0.09\%$. Once again, this is consistent with the stress not being fully relaxed during the 3-hr stress relaxation experiment.

Changes in the bulk density and total porosity due to stress relaxation for coatings in the as-sprayed and two heat-treated conditions are presented in Table 3. Note that for each case samples stress relaxed for 1200 °C/60 MPa/3 h are compared to samples that were only exposed to 1200 °C for 3 h. While the expected trends are apparent, i.e. reduced total porosity measured in samples that have been stress relaxed from 1200 °C/60 MPa as compared to those samples that have only been exposed to 1200 °C, the sensitivity of the Archimedes technique for samples with masses near 0.5 grams is too low to statistically separate the data points.

3.2. Stress relaxation effects on microstructure

Fig. 2 presents SEM images of a coating surface before and after stress relaxation at 1200 °C/60 MPa for 5 min. Note that micrographs are from identical regions in the sample and that a 1 h/1000 °C heat treatment was used to thermally etch the sample, revealing microstructural features. For these conditions, intralamellar cracks oriented perpendicular to the applied compressive stress were observed to permanently close after only 5 min of stress relaxation. Though not presented, there was no difference in crack width observed between the as-sprayed and 1 h/1000 °C HT condition when revisited prior to testing. The coatings surfaces presented in Fig. 2 show that cracks parallel to the applied load do not close while the perpendicular do, distinguishing the sintering process under the applied load from a normal sintering, which would show no preference to crack orientation.

To ensure the crack closure events were taking place during stress relaxation, and not during the initial monotonic loading ramp up to the constant applied strain, an as-sprayed coating was compressed monotonically up to the maximum stress of 60 MPa, i.e. a ~0.5% applied strain, at 1200 °C and then immediately unloaded. SEM investigations of the coating surface displayed no permanent crack closure perpendicular to the applied load for multiple areas revisited

Table 2
Change in the original height of stand-alone plasma-spray coatings due to stress relaxation from 60 MPa as a function of coating condition. The applied strain necessary to achieve a starting stress of 60 MPa in the sample is also shown. When the average ΔHeight is greater than the applied strain it suggests that the stress in the sample(s) was fully relaxed.

Coating condition	Stress relaxation parameters	Number samples	Average ΔHeight during relaxation (%)	Applied strain during relaxation (%)
As-sprayed	1200 °C/60 MPa/3 h	5	-0.75 ± 0.34	-0.46 ± 0.13
HT 50 h/1000 °C	1200 °C/60 MPa/3 h	4	-0.28 ± 0.09	-0.39 ± 0.15
HT 50 h/1200 °C	1200 °C/60 MPa/3 h	1	-0.18 ± 0.09	-0.28 ± 0.09

Table 3
Bulk density and total porosity values for coatings after heat treating or stress relaxation testing. The minimum uncertainty for a single bulk density and total porosity measurement for the setup utilized was determined to be 0.09 g/cm^3 and 1.5%., respectively.

Coating condition	Test parameters	Bulk density (g/cm^3)	Total porosity (%)	Number of samples
AS	1200 °C	5.52 ± 0.14	9.4 ± 2.3	95
AS	1200 °C/60 MPa/3 h	5.67 ± 0.09	6.8 ± 1.5	3
HT 50 h/1000 °C	1200 °C	5.51 ± 0.11	9.6 ± 1.8	6
HT 50 h/1000 °C	1200 °C/60 MPa/3 h	5.61 ± 0.09	7.9 ± 1.5	3
HT 50 h/1200 °C	1200 °C	5.56 ± 0.10	8.6 ± 1.6	20
HT 50 h/1200 °C	1200 °C/60 MPa/3 h	5.60 ± 0.09	7.8 ± 1.5	1

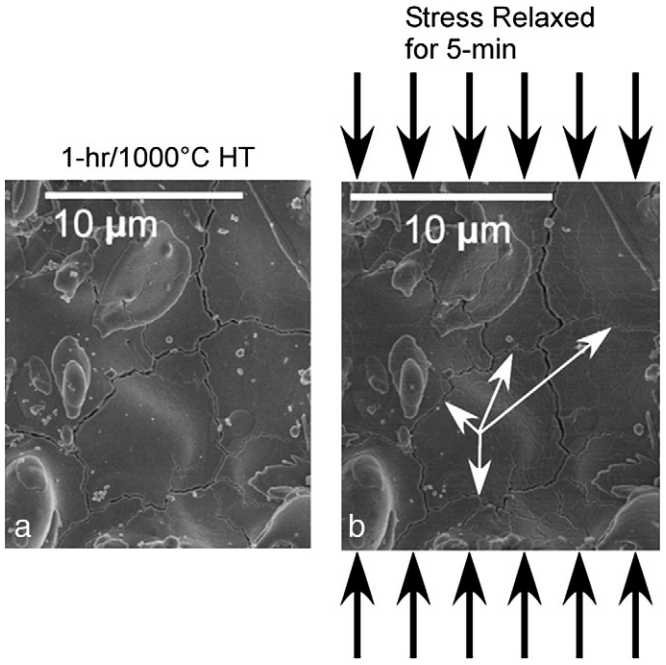

Fig. 2. SEM images of the surface of a plasma-sprayed stand-alone YSZ coating (a) prior to stress relaxation and (b) after 5 min of stress relaxation under a 60 MPa initially applied load at the test temperature of 1200 °C. The coating was heat-treated for 1 h/1000 °C prior to stress relaxation to aid in viewing grain boundaries. The arrows represent the direction of applied stress during testing; no load was applied during SEM imaging. Cracks perpendicular to the applied load decrease in width, while cracks parallel to the applied show no change or a slight widening in width. These data were generated on the ~600 μm thick coatings.

on the surface. Therefore it is likely that the observed *permanent* closure of the cracks occurred during relaxation and not the initial monotonic ramp up to the level of constant applied strain.

To determine if contributions from grain boundary sliding or grain deformation aided in stress relaxation, a coating heat-treated for 50 h/1000 °C then stress relaxed at 1200 °C/60 MPa for 3 h, was investigated. The 50 h/1000 °C coating condition was chosen as it afforded sharp grain boundary demarcation (see Fig. 3a). The area revisited after stress relaxation, presented in Fig. 3b, showed no grain deformation, further grain boundary grooving, and a very small amount of grain sliding. While grain boundary deformation has been observed [17] during creep experiments on stand-alone plasma-sprayed coatings for applied compressive strains of 3%, it was not observed for areas revisited in the current data set where compressive strains were well below 1%. Enhanced grain boundary grooving with increased temperature and time has been observed previously by Erk et al. [6]. For these stress relaxation conditions, an insignificant amount of grain boundary sliding was observed.

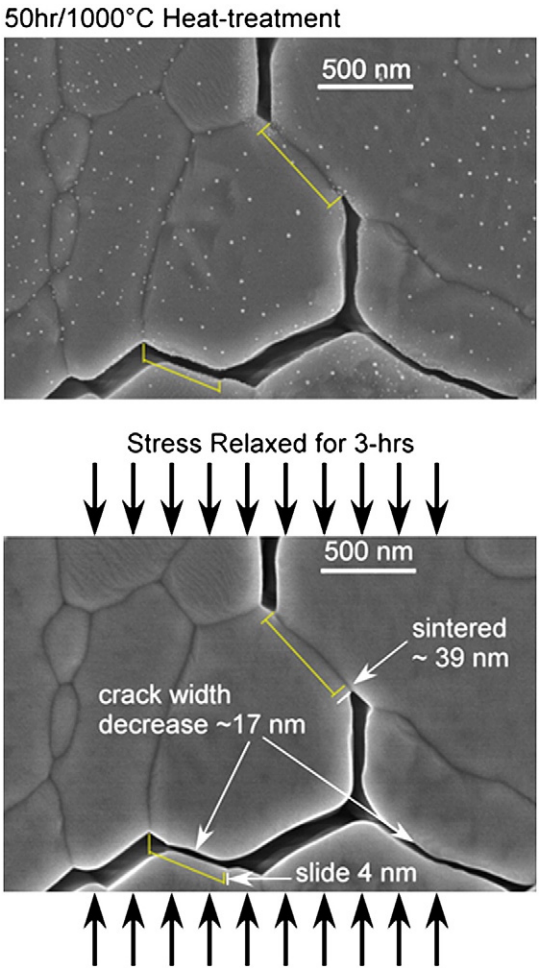

Fig. 3. SEM image of the surface of a YSZ coating (a) heat-treated for 50 h at 1000 °C, and then (b) stress relaxed at 1200 °C under the initially applied load of 60 MPa for 3 h. There was no observable change in grain dimensions or reorientation of one grain with respect to another. The crack oriented perpendicular to the applied load decreased in width approximately 17 nm. And a sliding of approximately 3–4 nm was observed for the top of the crack face relative to the bottom of the crack face with regards to the crack oriented perpendicular to the applied load. Sintering along the crack face, which occurred previously during the 50 h/1000 °C HT, was further promoted during stress relaxation at 1200 °C as the length of grain boundaries that chemically bound increased by approximately 39 nm in length. Overall the decrease in crack width perpendicular to the applied load is measurably larger than the sliding event or increase in width of the cracks oriented parallel to the applied load indicating a load orientation dependent deformation. These data were generated on the ~600 μm thick coatings.

Inspection of Fig. 3b did reveal further permanent closure of a crack oriented perpendicular to the applied stress, although the crack was not completely closed. Furthermore, sintering between two grains was observed to have occurred after stress relaxation. Only crack closure was directionally dependent upon the applied load; and is therefore a contributing strain exchange mechanism associated with the relaxation of APS coatings at high temperature.

3.3. Changes in internal void distribution specific surface area due to uniaxial stress relaxation

SANS measurements were used to quantify changes in the total specific surface area (SSA) of the voids as well as the specific surface areas of the two directionally oriented void systems, i.e. interlamellar pores and intralamellar cracks [28–31], and their changes due to stress relaxation at high temperature [5,20,22]. Fig. 4 shows a plot of the apparent Porod surface in one of the anisotropic cross sections, which is perpendicular to the spray direction, for as-sprayed, heat-treated, and stress relaxed coatings. Note the bulging disk shape that is associated with anisotropic scattering from the interlamellar pores (primarily at 0° and 180°) and intralamellar cracks (primarily at 90° and 270°). From the figure it is clear that there is a reduction in the apparent Porod surface with increasing temperature and/or stress application.

Isotropy of the scattering in the plane normal to the spray direction was confirmed by experiments even for the most severe test condition, i.e. stress relaxed at 1200 °C/60 MPa for 3 h. Because isotropic scattering in the plane normal to the spray direction was established for all coatings, it is valid to calculate the specific surface areas by integration about the isotropic (spray) direction. The uncertainty for SSA measurements made on plasma-sprayed void systems was established by a previous study to be about 0.1×10^6 m^2/m^3 [20], which will be applied as the error for a single measurement in the current study.

The SSA results of the ~600 μm thick coatings in the as-sprayed, stress relaxed (3 h/1200 °C/60 MPA), and heat-treated (3 h/1200 °C) conditions are shown in Fig. 5. The total void SSA in the as-sprayed condition is similar to previously reported values on plasma-sprayed coatings [5,20,22,32]. The total SSA of voids in the as-sprayed condition decreases when annealed at 1200 °C, either after heat treatment or

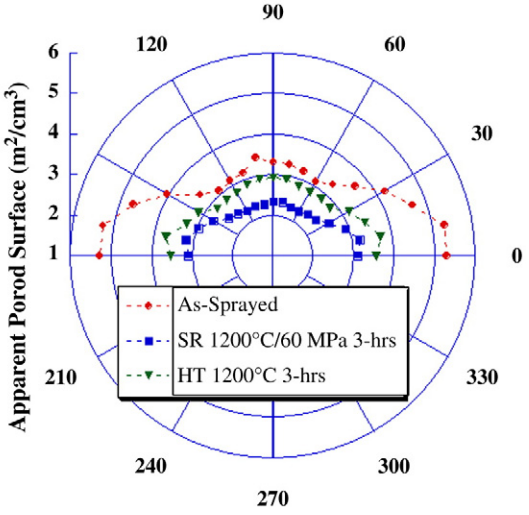

Fig. 4. 2D plot of azimuthal dependence of apparent Porod surfaces. The scattering cross-section was in an anisotropic plane normal to the spray direction. The data is from the ~600 μm thick YSZ coatings. The anisotropic scattering is clearly demonstrated by the directionality of the Porod surface as a function of the orientation angle. Note the bulging disk shape that is associated with anisotropic scattering from the interlamellar pores (primarily at 0° and 180°) and intralamellar cracks (primarily at 90° and 270°).

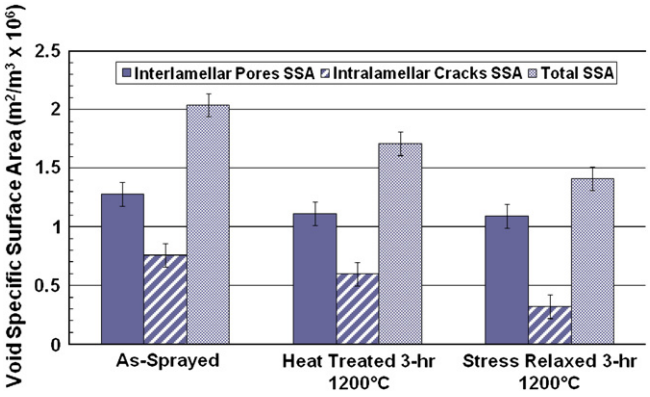

Fig. 5. Specific surface areas associated with individual void systems for as-sprayed, heat-treated, and stress relaxed 600 μm thick YSZ coatings. All stress relaxation tests began with an applied stress of 60 MPa. Note the main decrease in SSA observed for stress relaxed coatings is due to a decrease in the free surface associated with intralamellar cracks.

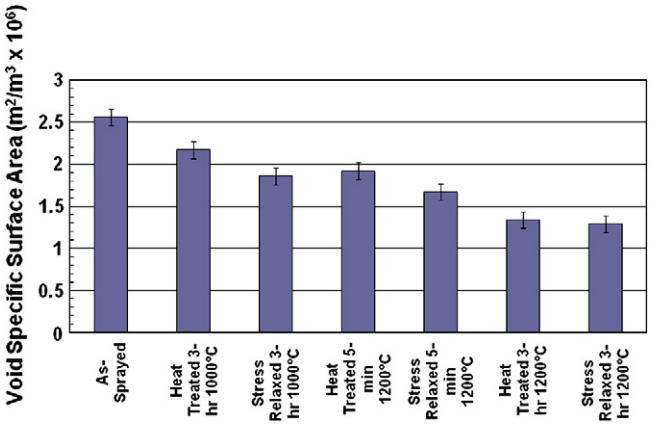

Fig. 6. Total SSA for 900 μm thick YSZ coatings subjected to various test conditions. Note that the total SSA decreases with increasing test temperatures and times. The starting stress was 60 MPa for all samples stress relaxed.

stress relaxation. Stress relaxation results in a discernable decrease in the total SSA of voids beyond an equivalent heat treatment at 1200 °C. Differentiation of the total SSA of the voids into contributions from interlamellar pores and intralamellar cracks identified a 47% difference in the SSA of intralamellar cracks between the stress relaxed and heat-treated coating conditions. A discernable change in the SSA of interlamellar pores was *not* observed between the stress relaxed and heat-treated coating conditions. Thus, the decrease in the total SSA of the voids for stress relaxed coatings can be attributed to principally the reduction of SSA of intralamellar cracks, which correlates directly with the observed permanent closure of intralamellar cracks at the surface by SEM.

The total SSA results of the ~900 μm thick coatings in various conditions are presented Fig. 6. In general, the total SSA of the voids systems decreases with increasing test temperature and time at temperature. For example, coatings stress relaxed at 1000 °C for 3 h show a 27% reduction in SSA when compared to the as-sprayed condition, while relaxation at 1200 °C for 5 min results in a 35% reduction in SSA compared to the as-sprayed condition. Similar to the 600 μm thick coating results, stress relaxation of the ~900 μm thick coatings results in lower SSAs for all test conditions when compared to the correlating heat-treatment condition with the exception of the samples tested at 1200 °C for 3 h. No statistical difference was noted between these two data sets.

It is worth noting that there was a difference in the SSA of the total voids of $\sim 0.5 \times 10^6$ m^2/m^3 between the 600 and 900 μm as-sprayed coating sets, indicating that these two coatings were not identical microstructurally. There are many plasma-spray variables that can change the resultant microstructure [1,12,33–35], and the current study attempted to keep the spray conditions and materials constant for each coating thickness. But, differences in the age of the cathode or anode can affect the plasma temperature, and therefore the substrate temperature and/or temperature of the melted droplets as they strike the substrate. For example, a hotter substrate temperature produces a coating with less fragmented or splashed lamellae, and a larger fraction of contiguous or disk-shaped lamellae [34,35]. Disk-shaped lamellae coatings result in reduced void specific surface area [35]. However, differences in the total void SSA were noted between samples heat-treated or stress relaxed for 5 min at 1200 °C that appeared to diminish with time at 1200 °C. Differentiation of the SSA contributions from intralamellar cracks and interlamellar pores for the 900 μm thick coating conditions resulted in ambiguous results, which suggest the true decrease in SSA of intralamellar cracks is masked by isotropic scattering due to globular pores or spherodized interlamellar pore free surfaces. For example, if interlamellar pores were to become more spherical then the scattering from their surfaces would become more isotropic and contribute to the SSA associated with intralamellar cracks, while reducing the percentage of SSA associated with interlamellar pores.

In summary, stress relaxation resulted in decreased SSA beyond an equivalent heat treatment for all conditions investigated with the exception of the 900 μm thick coatings after stress relaxation for 3 h/60 MPa/1200 °C. Relaxation at higher temperatures (1000 °C versus 1200 °C) and longer times (5 min versus 3 h) resulted in the greatest decreases in SSA. Differentiation of the SSA for void systems oriented parallel and perpendicular to the applied load isolated intralamellar crack closure as a physical change occurring in the APS microstructure during stress relaxation which exceeded that of an equivalent heat treatment but no stress applied.

3.4. Changes in thermal conductivity due to uniaxial stress relaxation

Thermal conductivity values, k_{th}, between 600° and 1200 °C for the as-sprayed, heat-treated condition of 1200 °C/3 h, and stress relaxed condition of 3 h at 1200 °C/60 MPa are presented in Fig. 7a. Stress relaxation of plasma-spray coatings resulted in increases in thermal conductivity beyond both the as-sprayed and heat-treated condition of 3 h at 1200 °C. The results for as-sprayed coatings stress relaxed for 5 min at 1200 °C under an initial load of 60 MPa versus the equivalent heat-treatment time of 5 min at 1200 °C, and the as-sprayed condition, are shown in Fig. 7b.

In comparing Fig. 7a and b it is apparent that the greatest increases in thermal conductivity occur during the initial 5 min of stress relaxation. For example, at 600 °C the k_{th} increases ~60% compared to the as-sprayed condition due to a 3-hr stress relaxation at 1200 °C. At the same measurement temperature a k_{th} increase of ~55% due to a 5-min stress relaxation at 1200 °C is noted; thus, there is only a 5% increase in k_{th} due to the extra 170 min at temperature under constant strain. Consequently, the first few minutes of relaxation decisively increases the k_{th} of APS coatings. Furthermore, a 5-min stress relaxation at 1200 °C increases the k_{th} more than 3 h of sintering at 1200 °C under no applied load.

Fig. 7c presents the k_{th} of as-sprayed coatings stress relaxed for 3 h at 1000 °C/60 MPa and heat-treated for 3 h at 1000 °C. This temperature is associated with microstructural coarsening, rather than densification, in plasma-sprayed YSZ [6]. Similar to the 1200 °C test data reported in Fig. 7a and b, the stress relaxed coatings tested at 1000 °C/60 MPa resulted in a higher k_{th} than an equivalent heat treatment for 3 h at 1000 °C (no applied strain). The coatings stress relaxed at 1000 °C/60 MPa display a lower thermal conductivity than the coating stress relaxed at 1200 °C/60 MPa, or heat-treated at 1200 °C for 3 h. The higher thermal conductivity for samples tested at

1200 °C compared to those stress relaxed at 1000 °C is linked to the densification occurring in the samples as a result of the higher stress relaxation temperature.

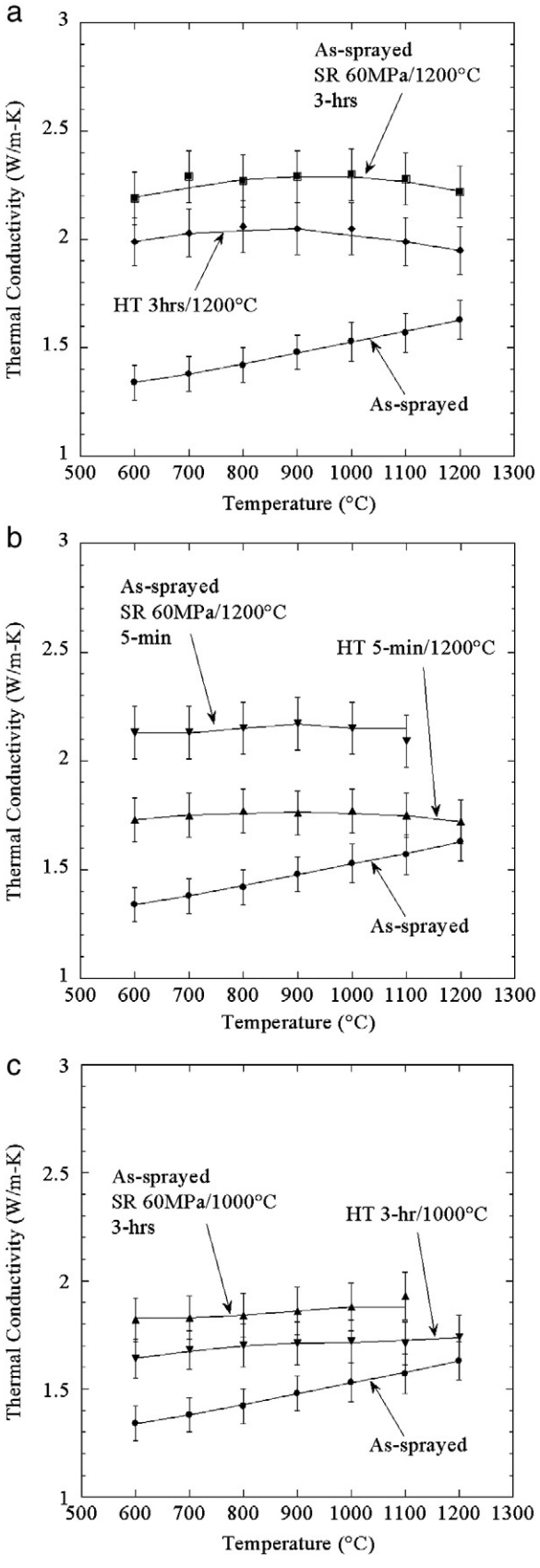

In summary, stress relaxed coatings display higher k_{th} values than their equivalent heat-treated coatings for the same duration at the same temperature. Thus, the thermal conductivity of plasma-sprayed YSZ is affected by both the test temperature and the applied strain during stress relaxation.

4. Discussion

4.1. Microstructural changes due to stress relaxation and effects on thermal conductivity

High-temperature stress relaxation in plasma-sprayed coatings *could* occur via several permanent deformation mechanisms, such as crack growth parallel to the applied load, permanent crack closure perpendicular to the applied load, lamellae sliding, or local plastic yielding at points of high stress concentration. Changes in the shape and amount of interlamellar pores and intralamellar cracks, along with grain sliding, were investigated presently.

Of the above listed stress relaxation mechanisms, the closure of intralamellar cracks perpendicular to the applied load was observed visually as shown in Figs. 2 and 3. Visual observation of crack closure was further quantified by SANS where the specific surface area of intralamellar cracks was reduced as a result of stress relaxation compared to coatings that were exposed only to temperatures (1200 °C). This data is presented in Fig. 5. While Fig. 5 showed that the SSA of the interlamellar pores trended downward with high-temperature exposure or high temperature and stress exposure, no statistical difference can be asserted. The same conclusion can be drawn from the Archimedes density data presented in Table 3. At the low applied strains, i.e. <1%, only minor grain boundary sliding was noted in the 3 h 1200 °C/60 MPa stress relaxation experiment (see Fig. 3) and further investigations would be necessary to isolate grain boundary sliding as a stress relaxation mechanism. Thus, the experimental evidence identifies the permanent closure of intralamellar cracks perpendicular to the applied load through pressure assisted sintering at crack faces in contact with one another is the primary mechanism by which stress is relaxed.

In this study the most extreme stress relaxation test condition was 3 h at 1200 °C from the initial applied stress of 60 MPa. For these experimental conditions, a measured permanent strain of $0.75 \pm 0.33\%$ was imparted on the coating due to relaxation and sintering combined. If the closure of intralamellar cracks is wholly responsible for the relaxation behavior, then the entire permanently imparted uniaxial strain of $0.75 \pm 0.34\%$ must be accommodated by an equal reduction in the porosity associated with the intralamellar crack closure. A multiple small angle neutron scatter (MSANS) study by Allen et al. [20] determined that intralamellar cracks account for ~22.8% of the total porosity in APS coatings sprayed from a fused and crushed powder similar to the morphology of the powder investigated currently. The total porosity of as-sprayed coatings in the current study was $9.4 \pm 2.3\%$, which correlates to ~2.1–2.2% of the total porosity residing as intralamellar cracks. Realizing that the entire

Fig. 7. (a) Thermal conductivity from 600° and 1200 °C for plasma-sprayed YSZ coating conditions of as-sprayed, heat-treated at 1200 °C/3 h, and stress relaxed for 3 h at 1200 °C/60 MPa. Standard deviations were calculated as a function of the each experimental measurement, i.e. α, ρ, and c_p, and replication between samples. Note the distinct increase in thermal conductivity due to stress relaxation, which exceeds the equivalent heat-treatment coating values. (b) Thermal conductivity from 600° and 1200 °C for plasma-sprayed YSZ coating conditions of as-sprayed, heat-treated at 1200 °C/5 min, and stress relaxed at 5 min at 1200 °C/60 MPa. Note the distinct increase in thermal conductivity due to stress relaxation for 5 min at 1200 °C, suggesting the greatest increases in thermal conductivity of plasma-sprayed coatings occurs very quickly during service. (c) Thermal conductivity from 600° to 1200 °C for plasma-sprayed YSZ coating conditions of as-sprayed, heat-treated at 1000 °C/3 h, and stress relaxed at 1000 °C for 3 h under an initially applied load of 60 MPa. All thermal conductivity data were generated on the ~600 μm thick coatings. The line is to guide the eye.

population of intralamellar cracks is not favorably oriented relative to the applied stress direction, only a percentage of the total crack population could physically contribute to the uniaxial change in height. Still, only 34–36% of *all* intralamellar cracks need to compact to accommodate the permanent strain. Arguably, the compaction and permanent closure of intralamellar cracks can accommodate stress relaxation in APS coatings below 1% compressive strains.

Finally, the combined effects of stress and temperature on thermal conductivity were greater than temperature alone (see Fig. 7). The microstructural reasons for the increase in k_{th} appears to be the reduced population of intralamellar cracks in stress relaxed coatings (see Fig. 5), caused by stress-enhanced sintering of cracks oriented perpendicular to the applied stress (Fig. 2). Comparison of Fig. 7a and b indicates that 5 min of stress relation at 60 MPa/1200 °C causes a great increase in thermal conductivity than 3 h at 1200 °C indicating that stress can have a large effect on k_{th} by more effectively and rapidly reducing the crack population.

4.2. Thermal conductivity as a function of specific surface area

The thermal conductivity of dense YSZ is a function of both phonon and photon transport, but for temperatures below 1200 °C where phonon conduction dominates, contributions from photons can be neglected [36–40]. As shown in Figs. 1–3, the plasma-spray process forms microstructures with large amounts of specific surface area per unit volume due to interlamellar pores and intralamellar cracks. This void microstructure lowers thermal conductivity values due to enhanced phonon scattering at YSZ/defect boundaries, and reduced conduction due to the low thermal conductivity of air contained in voids [41].

Models used to calculate k_{th} based solely on the amount of porosity do not adequately predict thermal conductivity values for plasma-sprayed coatings. For example, the Maxwell [42] and Klemens [43] approximations, which assume spherical pores, would predict thermal conductivities for YSZ with 9.4% porosity to be ~2.4 W/m K, while the as-sprayed microstructure with 9.4% total porosity was measured to be 1.3 W/m K, which is significantly lower. Furthermore, the same models would predict k_{th} values of ~2.5 W/m K for a porosity of 6.8%, a value similar to that observed for coatings subjected to stress relaxation at 1200 °C for 3 h under an initial applied stress of 60 MPa, while the measured value was 2.2 W/m K.

The lack of predictive capability of the current models stems from the spherical pore assumption. From a geometrical perspective, a spherical pore of some volume will have the minimum amount of surface area associated with it. High aspect ratio interlamellar pores and intralamellar cracks of the same volume as a spherical pore will have much larger specific surface areas [20]. Because the thermal conductivity of the plasma-sprayed coatings are significantly below the modeled values, it suggests that phonon scattering at free surfaces plays a large part in the actual thermal conductivity of plasma-sprayed coatings. A study by Z. Wang et al. [32] determined that free surfaces associated with air plasma-sprayed void systems decreased the intrinsic thermal conductivity of YSZ close to 60%. Thus, a relationship between thermal conductivity and the SSA associated with the plasma-sprayed void systems may demonstrate a stronger correlation than simply plotting k_{th} versus total porosity.

Fig. 8a and b plots the k_{th} values at 600 °C and 1100 °C from Fig. 7 versus the total SSA obtained from SANS experiments on as-sprayed, heat-treated and stress relaxed coatings. The k_{th} data displays an apparent linear relationship with the total SSA data for the analyzed temperatures of 600° and 1100 °C. The strongly correlated linear fit extrapolates to a thermal conductivity of ~2.8–3.0 W/m K for the fully dense 7 wt.% YSZ, which is in direct agreement with the thermal conductivity values reported in literature for a fully dense 6–8 wt.% Y_2O_3–ZrO_2 at 200 °C [37,40,44]. Similar results are noted for k_{th} values at 1100 °C as shown in Fig. 8b. While the linear curve fit is not a

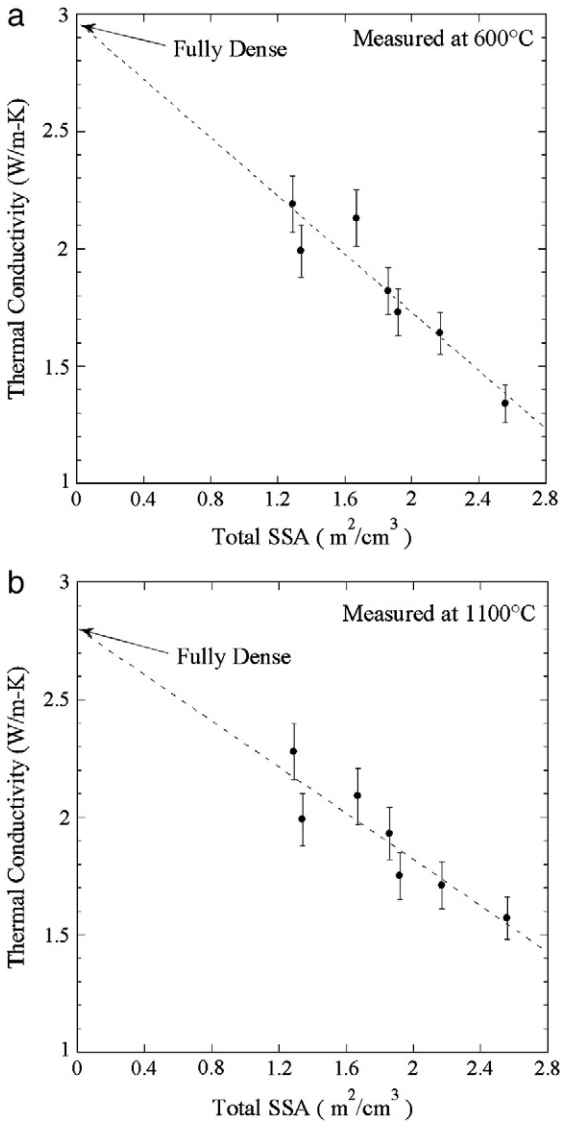

Fig. 8. (a) Thermal conductivity at 600 °C versus the total specific surface area of YSZ coatings in the as-sprayed, heat-treated or stress relaxed conditions. A linear curve fit extrapolated to zero SSA, i.e. a fully dense coating, results in a thermal conductivity consistent with reported values for YSZ. (b) Thermal conductivity at 1100 °C versus the total specific surface area of YSZ coatings in the as-sprayed, heat-treated or stress relaxed conditions, indicating similar trends to those observed at 600 °C.

physical model, it does suggest a linear relationship between the increase in SSA and the increase in thermal conductivity for YSZ plasma-sprayed coatings. For example, in Fig. 8a, an approximate 41% increase in thermal conductivity occurs as the SSA reduces from ~2.6×10^6 m^2/m^3 to 1.6×10^6 m^2/m^3, which is a ~38% change in SSA. The changes in k_{th} and SSA for the coating conditions measured are associated with a decrease in the total porosity of only ~2.6% or less.

The functional dependence of k_{th} and SSA is complicated and the data sets in the current study do not cover a large enough range of SSA to confidently assert thermal behavior for all plasma-sprayed coatings. A physical model would require the measurement of a SSA of a number an as-sprayed coating conditions and the correlating changes in SSA with temperature or temperature and stress application during the thermal conductivity measurements. Still, the data in the current study does suggest a direct dependence of k_{th} on the total SSA, which exceeds k_{th} dependence on porosity for the coating conditions characterized. Ultimately, understanding the effects of the evolving microstructure during stress relaxation on critical coating properties, for instance thermal conductivity will be key to future TBC development.

5. Conclusions

Stress relaxation behavior in plasma-sprayed YSZ coatings for applied strains below 1% at temperatures of 1000° and 1200 °C is controlled by permanent closure of intralamellar cracks via sintering of the free surfaces that are in contact as a consequence of the applied stress. The permanent closure of intralamellar cracks oriented perpendicular to the applied load at the surface of coatings was documented by SEM before and after testing. Stress relaxed coatings demonstrated a reduction in the SSA of void systems associated with intralamellar cracks that exceeded measured changes in SSA for coatings with equivalent heat treatments under no applied strain. The reduction in total SSA associated with stress relaxation has a direct effect on the thermal conductivity of the coatings. Decreases in total SSA were linked to increases in thermal conductivity, which demonstrated approximately linear correlation. The decrease in total SSA associated with stress relaxation at high temperature occurs very quickly. A ~35% decrease in SSA was observed after only 5 min of relaxation under an initial stress of 60 MPa at 1200 °C, which was tied to a ~55% increase in thermal conductivity. These results suggest that the thermal conductivity of thermal barrier coatings during initial service is actually higher than what is anticipated or reported due to application of service-induced compressive stresses.

Acknowledgements

Major portions of this research were funded by the National Science Foundation via grant DMR-0134286. Use of the Advanced Photon Source at the Argonne National Laboratory was supported by the U. S. Department of Energy, Office of Science, Office of Basic Energy Sciences, under contract no. DE-AC02-06CH11357. This project involved research sponsored by the Assistant Secretary for Energy Efficiency and Renewable Energy, Office of FreedomCAR and Vehicle Technologies, as part of the High Temperature Materials Laboratory User Program, Oak Ridge National Laboratory, managed by UT-Battelle, LLC, for the U.S. Department of Energy under contract number DE-AC05-00OR22725. The authors also wish to thank Dr. Boualem of NIST for his valuable contributions.

This research was based in part on the thesis submitted by C. Petorak for the Ph.D. Degree in Materials Engineering, Purdue University, West Lafayette, Indiana, 2007.

References

[1] R. McPherson, Surf. Coat. Technol. 39/40 (1989) 173.
[2] R. McPherson, Thin Solid Films 83 (1981) 297.
[3] R.A. Miller, Surf. Coat. Technol. 30 (1) (1987) 1.
[4] R.B. Heimann, Plasma-Spray Coatings: Principles and Applications, 1996 Weinheim, New York.
[5] J. Ilavsky, G.G. Long, A.J. Allen, C.C. Berndt, Mater. Sci. Eng. A272 (1999) 215.
[6] K.A. Erk, C. Deschaseaux, R.W. Trice, J. Am. Ceram. Soc. 89 (5) (2006) 1673.
[7] R.W. Trice, J. Su, J.R. Mawdsley, K.T. Faber, A.R. De Arellano-Lopez, H. Wang, W.D. Porter, J. Mater. Sci. 37 (2002) 2359.
[8] D. Zhu, R.A. Miller, J. Mater. Res. 14 (1) (1999) 146.
[9] E. Withey, C. Petorak, R. Trice, G. Dickinson, T. Taylor, J. Eur. Ceram. Soc. 27 (2007) 4675.
[10] G.R. Dickinson, C. Petorak, K. Bowman, R. Trice, J. Am. Ceram. Soc. 88 (8) (2005) 2202.
[11] Petorak, "Evolution of the Plasma-Sprayed Microstructure in 7 wt% Yttria-Stabilized Zirconia Thermal Barrier Coatings during Uniaxial Stress Relaxation and the Concomitant Changes in Material Properties," PhD. MSE Thesis, Purdue University (2007).
[12] R.A. Miller, J.Therm. Spray Technol. 6 (1) (1997) 35.
[13] W. Beele, G. Marijnissen, A. van Lieshout, Surf. Coat Technol. 120–121 (1999) 61.
[14] A.H. Bartlett, R. Dal Maschio, J. Am. Ceram. Soc. 78 (4) (1995) 1018.
[15] L. Singheiser, R. Steinbrech, W.J. Quadakkers, R. Herzog, Materials at High Temperatures 18 (4) (2001) 249.
[16] R. Herzog, P. Bednarz, E. Trunova, V. Shemet, R.W. Steinbrech, F. Schubert, L. Singheiser, Proceedings of the 30th International Conference and Exposition on Advanced Ceramics and Composites, Jan 22–27, 2006 Cocoa Beach, FL.
[17] R. Herzog, E. Trunova, R. Steinbrech, E. Wessel, R. VaBen, F. Schubert, L. Singheiser, International Conference on "Creep and Fracture in High Temperature Components — Design and Life Assessment Issues", Institution of Mechanical Engineers, Central London, UK, Sept 12–14, 2005.
[18] K. Kokini, A. Banerjee, T.A. Taylor, Mater. Sci. Eng. A 323 (2002) 70.
[19] K. Kokini, Y.R. Takeuchi, B.D. Choules, Surf. Coat. Technol. 82 (1996) 77.
[20] J. Allen, J. Ilavksy, G.G. Long, J.S. Wallace, C.C. Berndt, H. Herman, Acta Mater. 49 (2001) 1661.
[21] J. Ilavsky, P.R. Jemian, J. Appl. Cryst. 42 (2009) 347–353.
[22] J. Ilavsky, A.J. Allen, G. Long, S. Krueger, J. Am. Ceram. Soc. 80 (3) (1997) 733.
[23] ASTM C373-88, ASTM International, West Conshohocken, PA, USA.
[24] ASTM E1461-07, ASTM International, West Conshohocken, PA, USA.
[25] B. Nait-Ali, K. Haberko, H. Vesteghema, J. Absi, D.S. Smith, J. Eur. Ceram. Soc. 26 (2006) 3567.
[26] L.M. Clark III, R.E. Taylor, J. Appl. Phys. 46 (2) (1975) 714.
[27] W.D. Porter, Oak Ridge National Laboratory, differential scanning calorimetry data for ZrO_2 — 8 wt% Y_2O_3 made available to the authors, 2006.
[28] G.L. Squires, Introduction to Thermal Neutron Scattering, Cambridge University Press, 1978.
[29] R. Celotta, J. Levine, Methods of Experimental Physics — Neutron Scattering Volume 23 — Part A, Academic Press, Inc, Orlando, Fl, 1986.
[30] T. Chattarji (Ed.), Neutron Scattering from Magnetic Materials, Elsevier, Netherlands, 2006.
[31] R. Pynn, Neutron Scattering, A Primer, A Publication of Los Alamos Neutron Science Center (LANSCE), 1990.
[32] Z. Wang, A. Kulkarni, S. Deshpande, T. Nakamura, H. Herman, Acta Mater. 51 (2003) 5319.
[33] A. Kulkarni, A. Vaidya, A. Goland, S. Sampath, H. Herman, Mater. Eng. A359 (2003) 100.
[34] R. Ghafouri-Azar, S. Shakeri, S. Chandra, J. Mostighimi, Int. J. Heat and Mass Transf. 46 (2003) 1395.
[35] S. Sampath, X.J. Jiang, J. Matejicek, A.C. Leger, A. Vardelle, Mater. Sci. Eng. A272 (1999) 181.
[36] J.R. Nicholls, K.J. Lawson, A. Johnstone, D.S. Rickerby, Surf. Coat Technol. 151–152 (2002) 383.
[37] P.G. Klemens, M. Gell, Mater. Sci. Eng. A245 (1998) 143.
[38] K. Schlichting, N. Padture, P. Klemens, J. Mater. Sci. 36 (2001) 3003.
[39] M.R. Winter, D.R. Clarke, J. Am. Ceram. Soc. 90 (2) (2007) 533.
[40] S. Raghavan, H. Wang, R.B. Dinwiddie, W.D. Porter, M. Mayo, Scr. Mater. 39 (8) (1998) 1119.
[41] R. McPherson, Thin Solid Films 112 (1984) 89.
[42] J.C. Maxwell, A Treatise on Electricity and Magnetism, Clarendon Press, Oxford, UK, 1904.
[43] P.G. Klemens, High Temps. High Press 23 (3) (1991) 241.
[44] J.F. Bisson, D. Fournier, J. Am. Ceram. Soc. 83 (8) (2000) 1993.